Shi a. G B (2020) 21:120
https://doi.org/10.1186/s13059-020-02022-2

Genome Biology

RESEARCH Open Access

Results

The RNA structure landscape during zebrafish early embryogenesis revealed "hot" structurally variable sites enriched with *cis*-regulatory elements

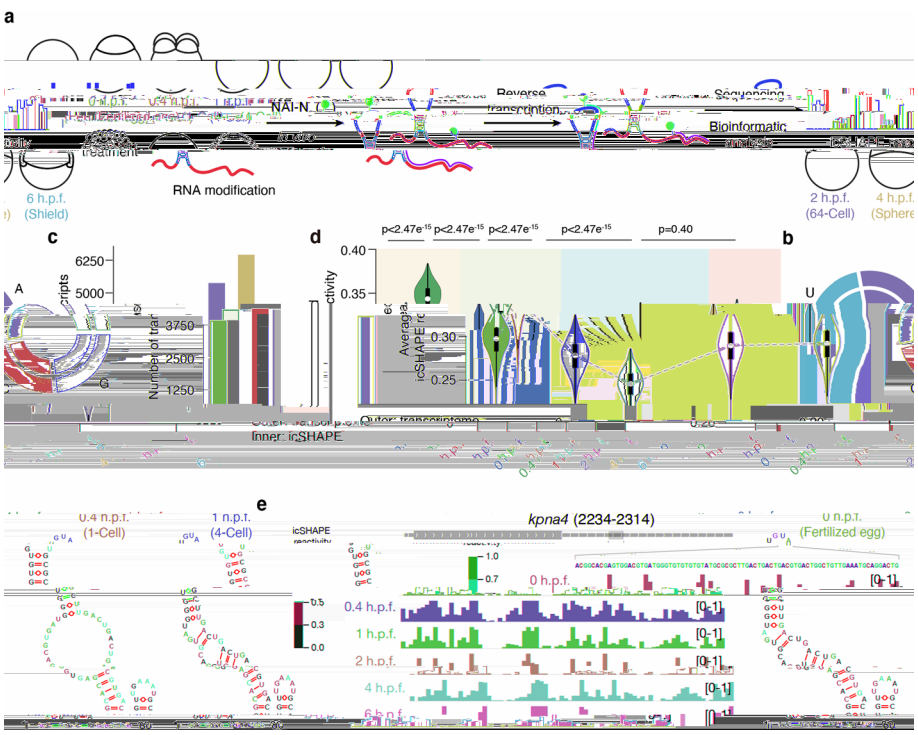

Fig. 1 Comprehensive RNA structural maps during zebrafish early embryogenesis. **a** Schematic view of in vivo RNA structural maps during zebrafish early development using icSHAPE. **b** Nucleotide composition in transcriptome and all profiled sites (transcriptome, A: 27.91%, U: 25.96%, C: 22.47%, G: 23.66%; icSHAPE, A: 27.86%, U: 25.99%, C: 22.37%, G: 23.78%). **c** The number of transcripts with more than half of the nucleotides with valid structural signals at each stage. **d** Global structural changes by violin plot of average icSHAPE reactivity of each transcript during zebrafish early development; *P* values were calculated by paired two-sided Student's *t* test. **e** Integrative Genomics Viewer (IGV) view of icSHAPE reactivity and RNA structure model of *kpna4* gene at 3′ UTR region

( )

kpna4

( )

(

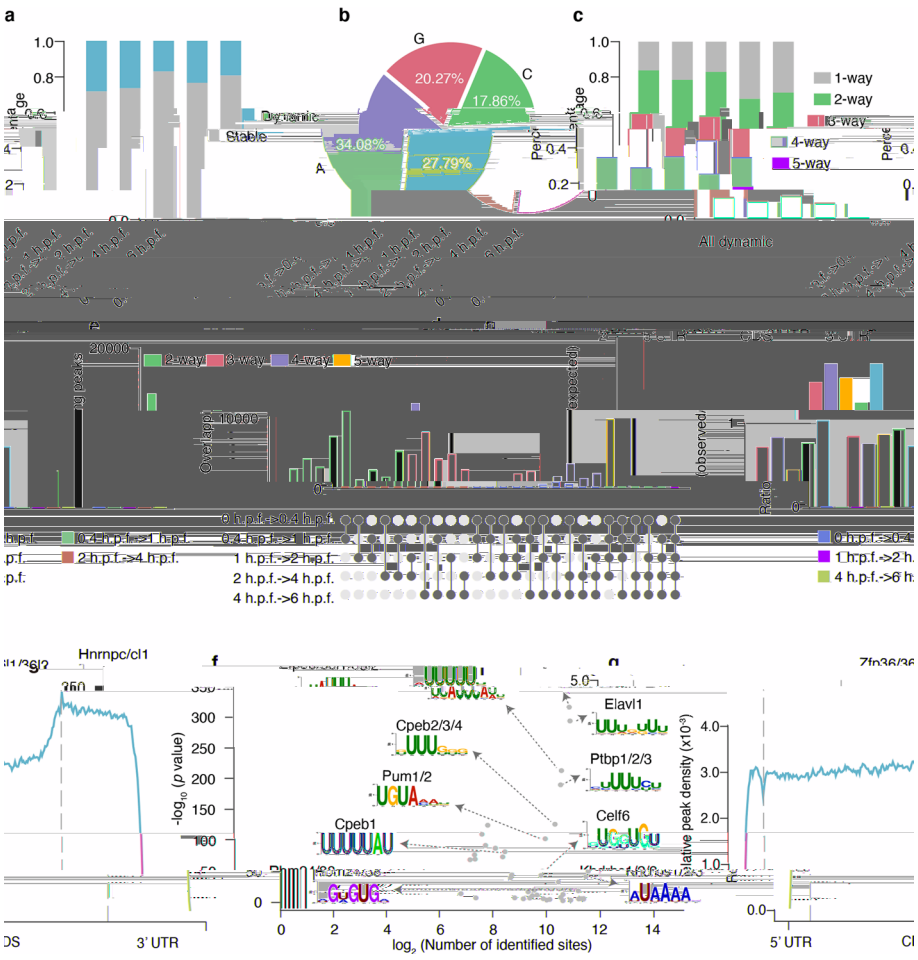

Fig. 2 Hot structurally variable sites enriched with *cis*-regulatory elements. **a** Distribution of structurally variable nucleotides between adjacent developmental stages. **b** Nucleotide composition of all structurally variable nucleotides. **c** The distribution of common (2,3,4,5-way) or specific (1-way) structurally variable regions in different comparisons. The structurally variable region that is specific to one comparison is termed as "1-way," while 2-way means that the structurally variable regions is shared by two comparisons, 3-way means that it is shared by three comparisons, and so on. **d** The statistics of all structurally variable regions grouped by their commonality. **e** Ratio of observed counts and expected counts of all structurally variable windows in three segments: 5′ UTR, CDS, 3′ UTR. The ratio is calculated by observed counts divided by expected counts. Statistical significance of enrichment of structurally variable windows in 3′ UTR was carried out with Fisher's exact; *P* value $< 2.23 \times 10^{-308}$ for all comparisons. **f** Metagene profile depicts the sub-transcript distribution pattern of common structurally variable regions shared by at least two comparisons. **g** Scatter plot shows the significance and occurrences of RNA-binding motif enriched in common structurally variable regions at 3′ UTR shared by at least two comparisons. *P* values were calculated by Fisher's exact test. Refer to method section "De novo motif discovery and enrichment analysis of structurally variable regions"

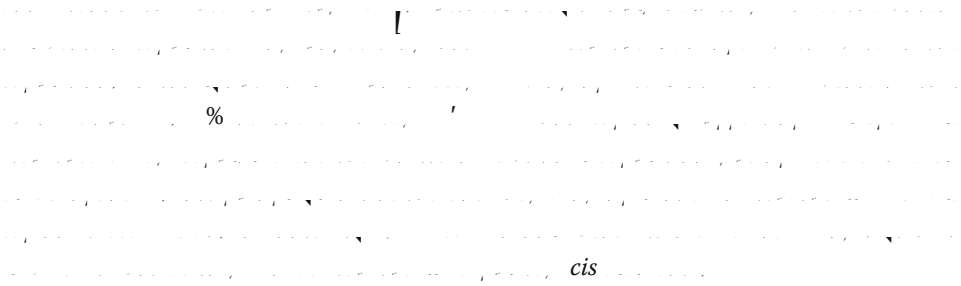

Elavl1a is enriched in variable structural regions in 3′ UTRs and prefers to bind single-stranded RNA in vivo and in vitro

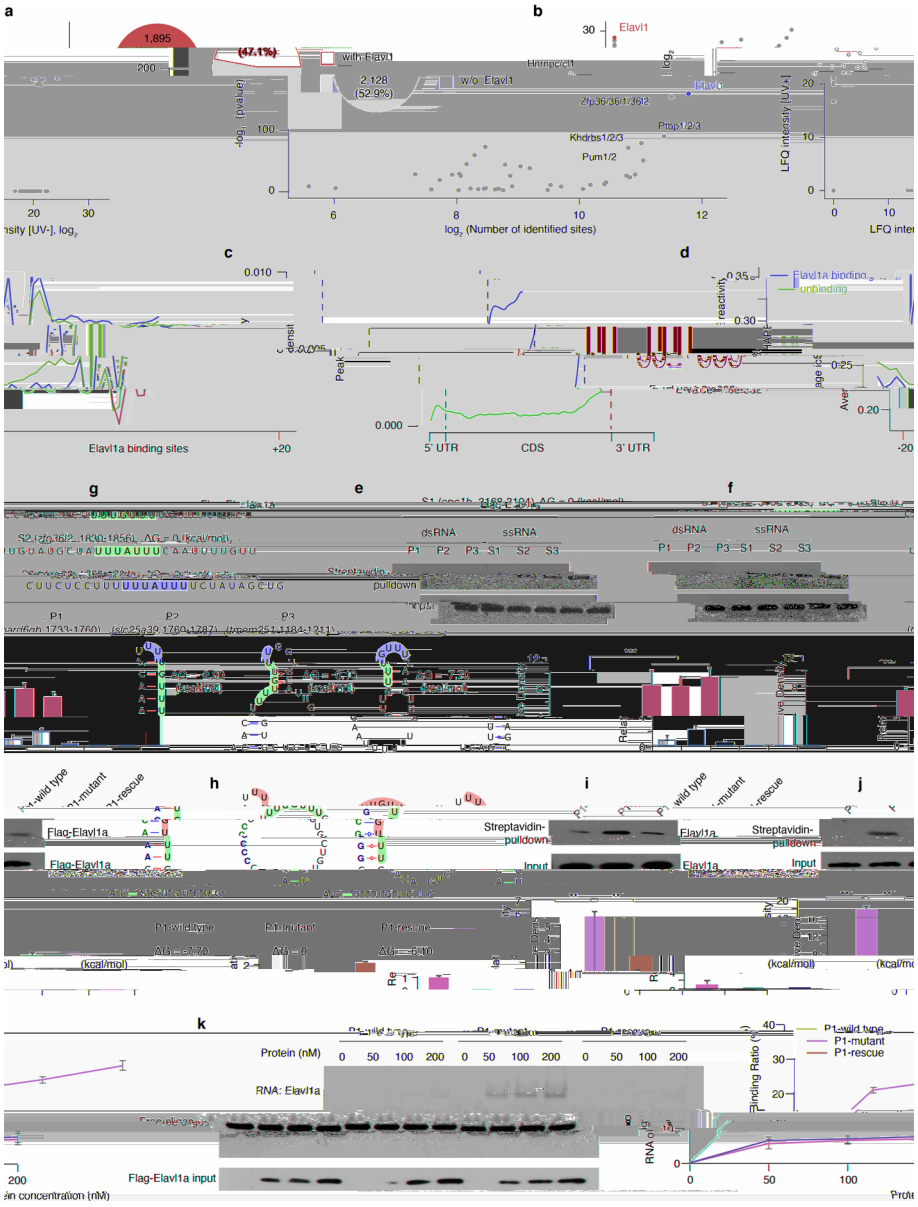

Fig. 3 (See legend on next page.)

(See figure on previous page.)
Fig. 3 Elavl1a prefer to bind single-stranded RNA in vivo and in vitro which enriched in structurally variable regions in 3′ UTRs. **a** Scatter plot shows the significance and occurrence of RNA-binding motif enriched in structurally variable windows at 3′ UTR between 4 h.p.f. and 6 h.p.f.; *P* values were calculated by Fisher's exact test. Inner pie chart shows 47.1% of transcripts with structurally variable regions at their 3′ UTR containing Elavl1 binding motif. **b** Scatter plot shows Elavl1a's enrichment in UV (+) sample at 4 h.p.f.. LFQ, label free quantitation. **c** Distribution of Elavl1a peaks across the length of mRNA and binding motif identified by Dreme (MEME suite) with Elavl1a-binding peaks in 3′ UTR (*E*-value = 1.8×10^{-332}). **d** icSHAPE metaprofile around Elavl1a binding sites and unbound sites with the same motif shows that Elavl1a tend to bind ssRNA in vivo. **e** The structure models of six endogenous RNA probes containing Elavl1a binding sites. Elavl1a binding sites were colored in red background. **f** Demonstration of endogenous Elavl1a pulled down by endogenous RNA probes containing Elavl1a binding sites. Upper, western blotting; lower, quantification level. Error bars, mean ± s.d., $n = 3$. *P* values were calculated using Student's *t* test. **g** Demonstration of purified Flag-Elavl1a pulled down by endogenous RNA probes containing Elavl1a binding sites. Upper, western blotting; lower, quantification level. Error bars, mean ± s.d., $n = 3$. *P* values were calculated using Student's *t* test. **h** The structure models of designed P1 wild-type, P1 mutant, and P1 rescue RNA probes containing Elavl1a binding sites and flanking regions. **i** Demonstration of endogenous Elavl1a pulled down by designed endogenous RNA probes containing Elavl1a binding sites. Upper, western blotting; lower, quantification level. Error bars, mean ± s.d., $n = 3$. *P* values were calculated using Student's *t* test. **j** Demonstration of purified Flag-Elavl1a pulled down by designed endogenous RNA probes containing Elavl1a binding sites. Upper, western blotting; lower, quantification level. Error bars, mean ± s.d., n = 3. *P* values were calculated using Student's *t* test. **k** EMSA (left) and line graph quantification (right) showing the binding ability of purified Flag-Elavl1a with designed P1 wild-type, P1 mutant, and P1 rescue RNA probes containing Elavl1a binding sites. In total, 100 nM of RNA probes was incubated with different concentrations of Flag-Elavl1a protein. The RNA binding ratio was calculated by (RNA protein) / ((free RNA) + (RNA protein)). Error bars, mean ± s.d., $n = 3$

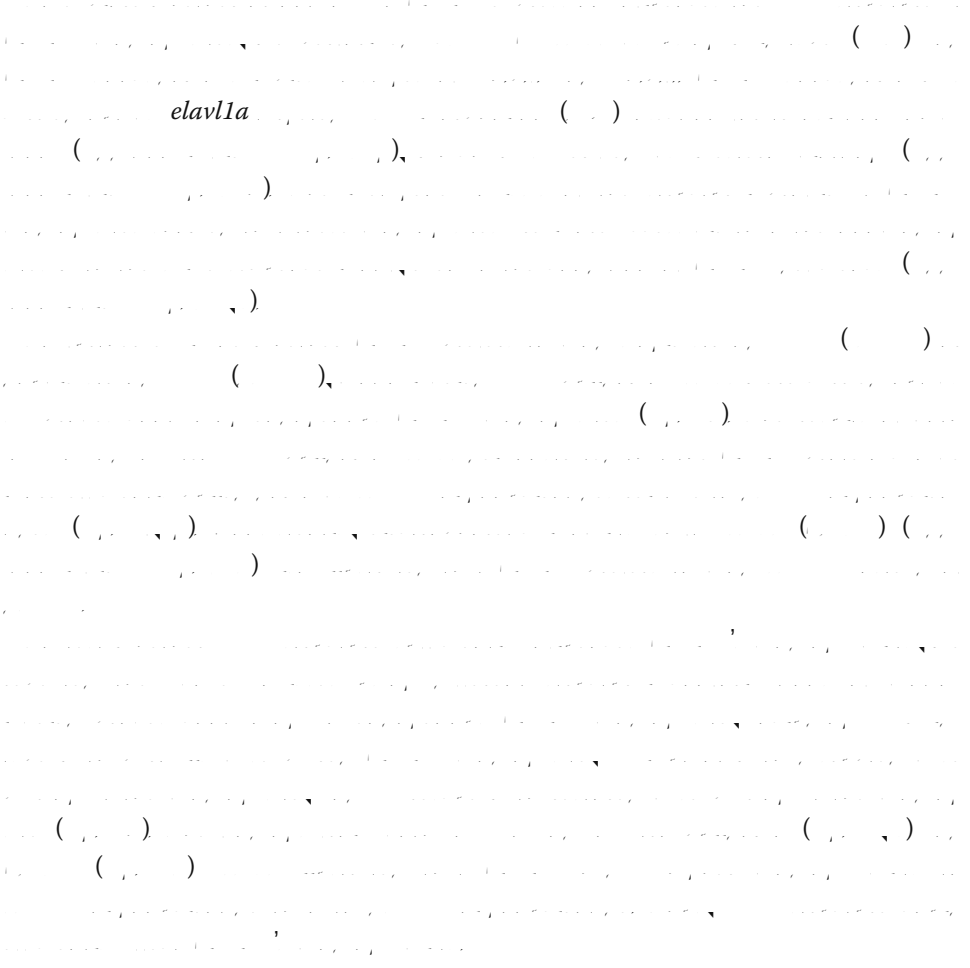

RNA structurally variable elements in Elavl1a binding regions correlate with maternal RNA stability

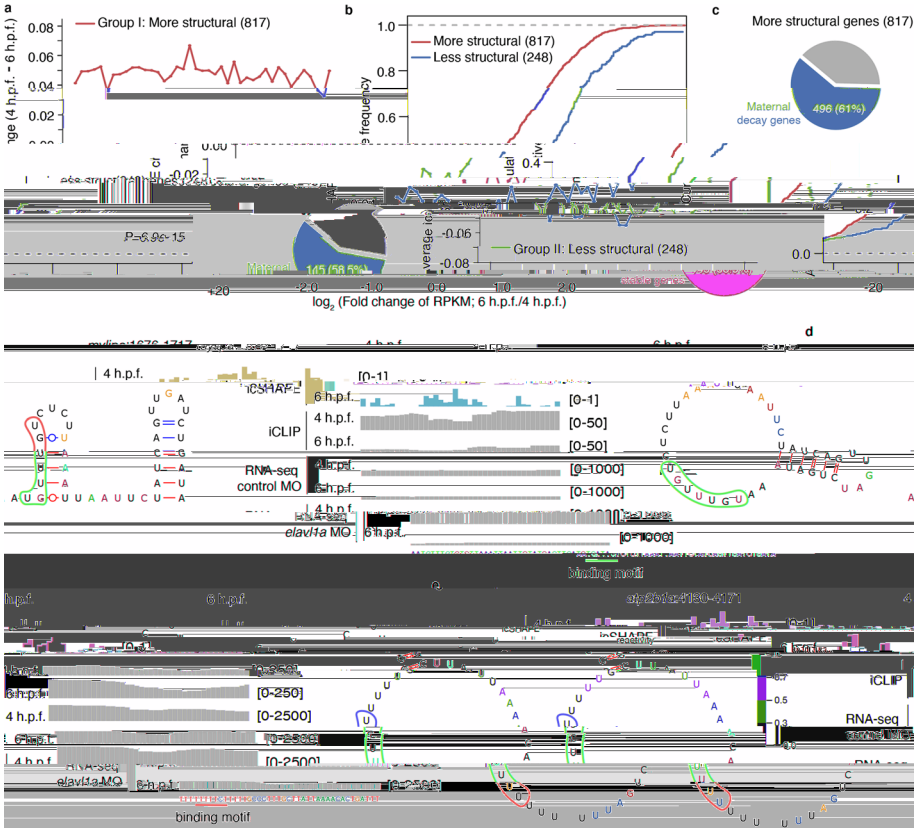

Fig. 4 RNA structurally variable elements in Elavl1a binding regions associate with maternal RNA stability. **a** Average icSHAPE reactivity change (4 h.p.f. and 6 h.p.f.) at the Elavl1a binding site of the two groups of transcripts. Group I: more structural, forming more structure at Elavl1a binding sites. Group II: less structural, forming less structure at Elavl1a's binding sites. "More structural" group was defined as the average of icSHAPE reactivity of those Elavl1-binding sites at 6 h.p.f. is less than that at 4 h.p.f. and the differences were larger than 0.05 (lower icSHAPE reactivity indicates that RNA structure become less accessible to SHAPE reagent, thus become more compact structure). Statistical significance was calculated by paired *t*-test and set to be $P < 0.05$. While the "less structural" group is defined as the average of icSHAPE reactivity of those Elavl1-binding sites at 6 h.p.f., it was larger than that at 4 h.p.f. and the difference is also larger than 0.05, $P < 0.05$. **b** Cumulative distribution of the $\log_2$ fold changes of the RNA level between two group transcripts with more or less structural Elavl1a binding sites during the period of 4 h.p.f. to 6 h.p.f.. *P* value was calculated using two-sided Wilcoxon test. **c** Pie chart depicting the proportion of maternal decay genes in transcripts with more structural Elavl1a binding sites, and the proportion of maternal stable genes in transcripts with less structural Elavl1a binding sites during the period of 4 h.p.f. to 6 h.p.f.. **d, e** IGV tracks and structure profile displaying icSHAPE (upper panels), iCLIP-seq (middle panel), and RNA-seq (bottom panel) read distributions in 3′ UTR of *mylipa* (**d**) and *atp2b1a* (**e**) mRNA. Binding motifs are indicated with red highlight

( )

" "

Elavl1a-mediated mRNA stability is required for early development

elavl1a
elavl1a ( )

elavl1a ( ) *elavl1a*
( )
elavl1a
( )
elavl1a
(*elavl1a*⁻ ⁻) (*elavl1a* ⁻) ( )
elavl1a
elavl1a *elavl1a*
elavl1a (
)
(
)
elavl1a (
)
(*P* ⁻),
(*P* ⁻)
( )

Elavl1a regulates maternal RNA stability in a structure-dependent fashion

( )
(*pard6gb*)
( )
( )

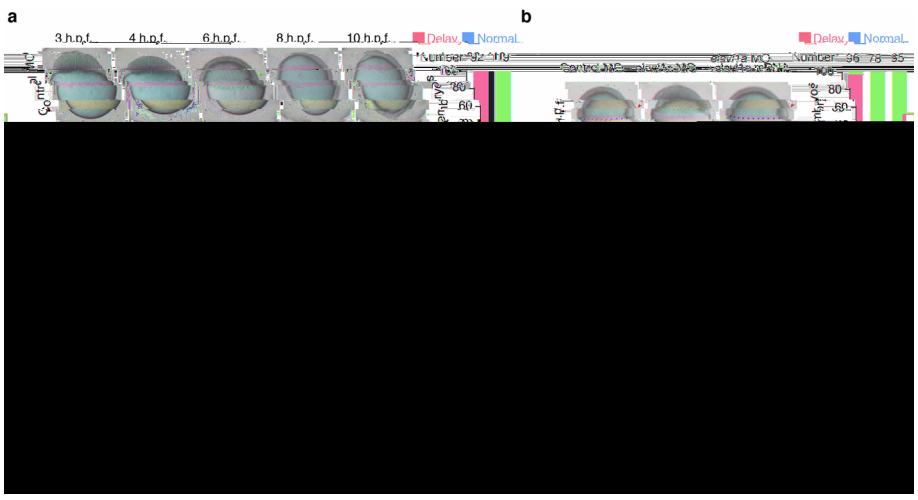

Fig. 5 Developmental delay and accelerated maternal RNA clearance induced by Elavl1a deficiency. **a** Elavl1a deficiency leads to developmental delay during zebrafish early embryogenesis. **b** Zebrafish *elavl1a* mRNA with MO-mismatch binding site can partially rescue the phenotype in *elavl1a* morphants. **c** Cumulative distribution of the $\log_2$ fold changes of RNA level between control and *elavl1a* morphants during the period of 4 h.p.f. to 6 h.p.f.. *P* values were calculated by two-sided Kolmogorov-Smirnov test. **d** Cumulative distribution of the $\log_2$ fold changes of RNA level of *elavl1a* morphants versus control in maternal decay, maternal stable and zygotic groups at 6 h.p.f.. *P* values were calculated by two-sided Kolmogorov-Smirnov test. **e** Gene set enrichment analysis of downregulated genes upon Elavl1a deficiency

( ) ( )

elavl1a

( ) *elavl1a*

( )

( ) *elavl1a* ( )

( )

( )

Discussion

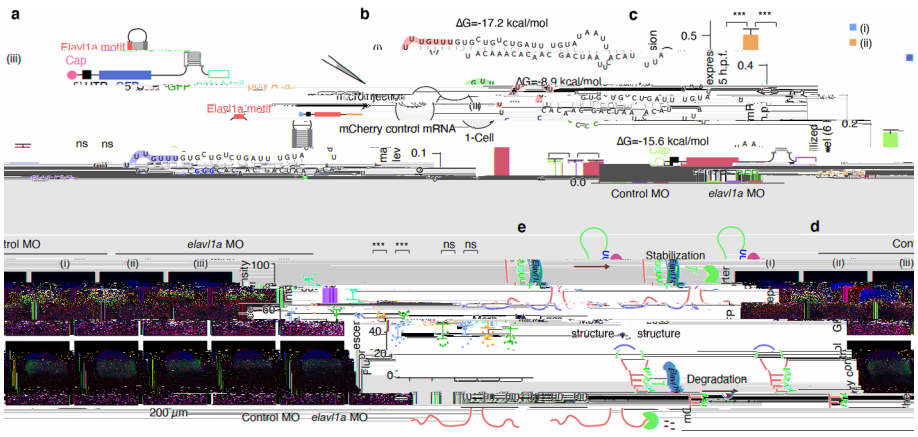

Fig. 6 Elavl1a regulates maternal RNA stability in a structure-dependent fashion. **a** Design of the GFP reporter mRNA with single-stranded or double-stranded Elavl1a binding site in its 3′ UTR. **b** The structure models of designed (i) wild-type, (ii) mutant, and (iii) rescue Elavl1a binding sites and flanking regions. **c** The relative mRNA level (6 h.p.f. versus 0.5 h.p.f.) of reporter genes with different structural contexts of Elavl1a binding motif in control and *elavl1a* morphants, $n = 3$ for each group, error bars, mean ± s.d.; *P* values were determined by two-sided Student's *t* test. **d** The protein level of reporter gene with different structural contexts of Elavl1a binding motif at 6 h.p.f. in control and *elavl1a* morphants determined by GFP fluorescence signal observation. Some pictures of representative embryos were shown. Quantitative fluorescence intensity was shown on the right, $n = 20$ for each group. Error bars, mean ± s.d. *P* values were determined by two-sided Student's *t* test. **e** Schematic model shows that Elavl1a regulates RNA stability in a structure-dependent fashion

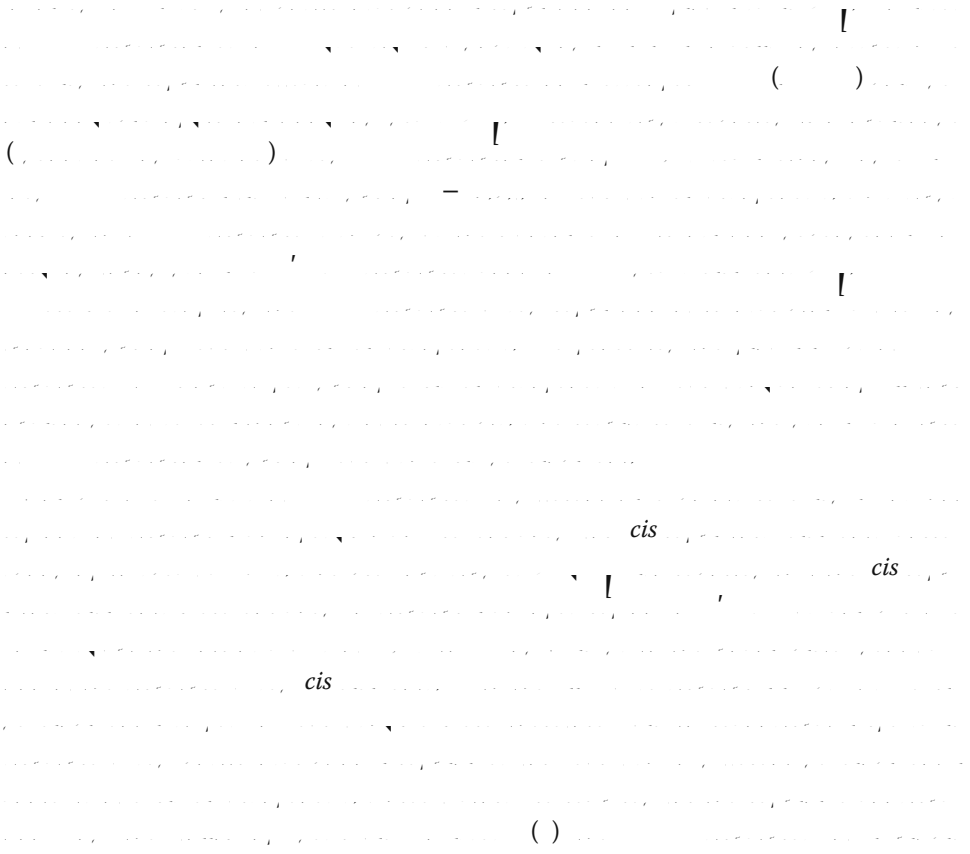

( )

( )

( )

Drosphila

( )

Methods

Animal models

Cell lines

( )

( ) %

( ) ( ) %

Morpholinos, vector construction, mRNA synthesis, injection

( ) *elavl1a* ′ ′ ′ (*elavl1a*、) *elavl1a* 、*myc* *flag* *elavl1a* ™ ( ) ™ ( ) ( ) ′

Generation of mutant by CRISPR/Cas9

elavl1a ! ( ) ( ) *elavl1a* ( )

Microscopy

Whole-mount in situ hybridization

( ) ′ ( ) *elavl1a* *elavl1a* 、*elavl1a* ( )、 ( ) ( )、 ( )

Western blotting

(–)、 β ! ( )、 ( )

Manual SHAPE analysis

In vivo SHAPE modification

icSHAPE deep-sequencing library preparation

Elavl1a iCLIP

flag-elavl1a

RNA-seq

Elavl1a RIP

myc-elavl1a

In vivo isolation of mRBPs from zebrafish embryos

Protein purification in mammalian cells

In vivo RNA pulldown assay

In vitro RNA pulldown assay

( ) (% μ)

™ ( ) ( )

™ – % ( ),

(,)

Electrophoretic mobility shift assay (EMSA)

μ , μ , μ , μ (,

, % , , % ,

, μ) ( )

) μ (, , , ,)

μ (%) μ

μ % (,)

(( ) (( )) ( ))

(–)

Identification of structurally variable nucleotides and regions and “hot” structurally variable sites

l

%

( ) Δ

Δ %

Δ

' t P

Δ P (' t)

( )

≥ %

P (' t) – P

“ ”

“ ”

“ ”

Enrichment of structurally variable regions in different parts of transcripts

' ' '

' ( ), ( ), '

( ) (–)

l

De novo motif discovery and enrichment analysis of structurally variable regions

De novo motif discovery in structurally variable regions

RBP binding motif enrichment analysis

Data processing and peak calling of iCLIP

Preprocessing and peak calling

Binding motif identification

Gene ontology analysis

( ) ( )

Analysis of the icSHAPE reactivity at zebrafish RBP binding sites

( )

%

Quantification and statistical analysis

' t

P

P

' P – ( )

' t P

( )

'

dgcr8 ' t

n , *n* P ( )

P

( )

'

' P P

– ( )

' P ( ) P

' t (*n*) , P , P , P ( )

P ( )

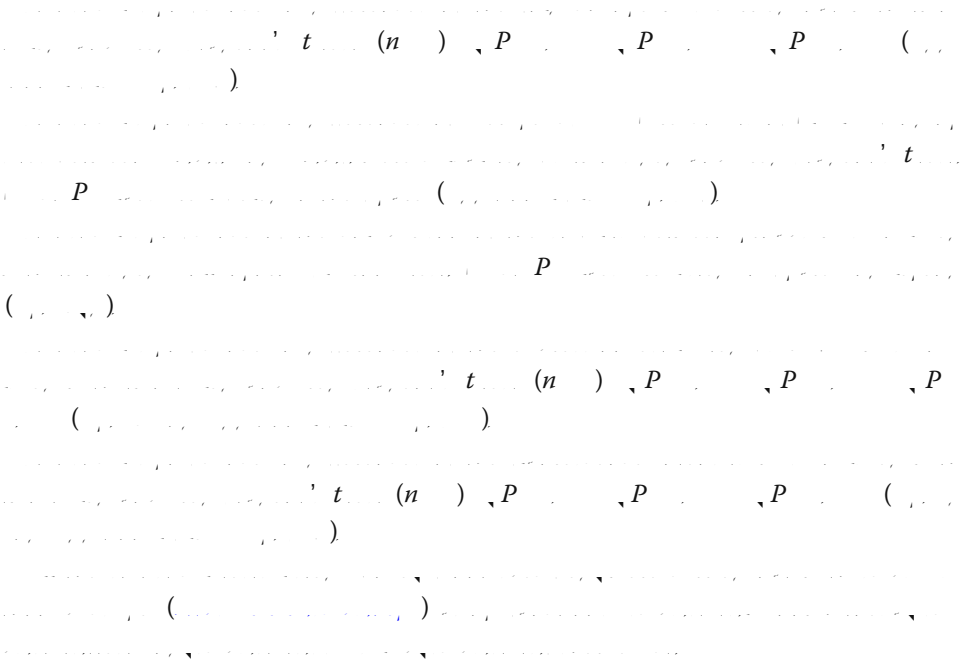

Supplementary information

Supplementary information accompanies this paper at https://doi.org/10.1186/s13059-020-02022-2.

Additional file 1: Supplementary Figures S1-S7.

Additional file 2: Table S1. Summary and statistics of icSHAPE, RNA-seq and iCLIP.

Additional file 3: Table S2. LFQ intensity of proteins in UV+ and UV- samples at 0, 0.4 and 4 h.p.f.

Additional file 4: Table S3. Structurally variable regions between neighboring stages and hot structurally variable regions.

Additional file 5: Table S4. Results of motif enrichment analysis in 3′ UTR structurally variable regions.

Additional file 6: Table S5. Summary of DLE element in structurally variable regions during early development and its associated biological function.

Additional file 7: Table S6. Elavl1a binding sites at 4 h.p.f. Elavl1a binding sites identified by Flag-Elavl1a iCLIP at 4 h.p.f. and 6 h.p.f.

Additional file 8: Table S7. Maternal and zygotic gene sets categorized by gene expression and SNP.

Additional file 9: Table S8. GO term enrichment analysis of down-regulated genes upon elavl1a knockdown at 6 h.p.f.

Additional file 10: Table S9. List of oligos used for this Study.

Additional file 11: Review history.

Acknowledgements

We thank Jifeng Wang and Mengmeng Zhang at laboratory of Proteomics, core facility in the Institute of Biophysics, CAS for their technical support of LC-MS analysis, and BIG CAS genomic platform for sequencing.

Review history

The review history is available as Additional file 11.

Peer review history

Barbara Cheifet was the primary editor on this article and managed its editorial process and peer review in collaboration with the rest of the editorial team.

Funding

This work was supported by grants from the National Natural Science Fund for Distinguished Young Scholars (31625016), the Strategic Priority Research Program of the Chinese Academy of Sciences, China (XDA16010501, XDA16010104), the National Natural Science Foundation of China (31425016, 91740204, 31871311, 31830061 and 31671355), CAS Key Research Projects of the Frontier Science (QYZDY-SSW-SMC027), K.C.Wong Education Foundation, Shanghai Municipal Science and Technology Major Project (2017SHZDZX01), the National Key Research and

Development Program of China (2018YFA0800200), the National Basic Research Program of China (2019YFA0110002) and the NSFC consulting grant (91940000).

Availability of data and materials

The RNA-Seq, iCLIP, and icSHAPE data supporting the conclusions of this article has been deposited in the Gene Expression Omnibus database under accession number GSE120724 [64], and also the Genome Sequence Archive [65] under accession number CRA001139 [66] linked to the project PRJCA001046.
The ribosome profiling data for zebrafish embryos at 2 and 6 h.p.f. was obtained from Gene Expression Omnibus database under accession number GSE52809 (https://www.ncbi.nlm.nih.gov/geo/query/acc.cgi?acc=GSE52809) (Subtelny et al., 2014) [67].
The human ELAVL1 binding sites was obtained from (https://www.cell.com/cms/10.1016/j.molcel.2011.06.008/attachment/51bc4461-fc31-4e4d-9b6d-c0db20a7e62b/mmc3.xls) (Lebedeva et al., 2011) [43] and (https://www.cell.com/cms/10.1016/j.molcel.2011.06.007/attachment/ed673aa9-bc87-4a4e-94b9-64fbaa1a6f61/mmc3.zip) (Mukherjee et al., 2011) [39].
The zebrafish iCLIP dataset for 23 RBPs was obtained from (https://track.giraldezlab.org/vejnar_et_al_2019_genome_research_iclip/danRer11/) (Vejnar et al., 2019) [32].
The gene set with maternal and paternal SNP information was collected from (http://dev.biologists.org/lookup/suppl/doi:10.1242/dev.095091/-/DC1, Harvey et al. 2013) [44].
The source code to reproduce all figures in this study are available on Github repository at site [68] and Zenodo [69].

Authors' contributions

B.Y.S. and J.S.Z. performed most of the experiments with assistance from Y.Y., N.Z., and H.L.W.; J.G. and T. Z performed bioinformatics analysis with help from P.L. and B.F.S.; J.H. performed experiments in zebrafish.; Y.G.Y., Q.C.Z., and F.L. conceived this project, supervised the study and interpreted the data, and wrote the manuscript with assistance from Z.Y.L., J.S.Z., J.H., J.G., and B.Y.S. The authors read and approved the final manuscript.

Ethics approval and consent to participate

Animal experimentation: This study was approved by the Ethical Review Committee in the Institute of Zoology, Chinese Academy of Sciences, China.

Competing interests

The authors declare that they have no competing interests.

Author details

[1]CAS Key Laboratory of Genomic and Precision Medicine, Collaborative Innovation Center of Genetics and Development, College of Future Technology, Beijing Institute of Genomics, Chinese Academy of Sciences, Beijing 100101, China. [2]University of Chinese Academy of Sciences, Beijing 100049, China. [3]MOE Key Laboratory of Bioinformatics, Center for Synthetic and Systems Biology, Beijing Advanced Innovation Center for Structural Biology, Tsinghua-Peking Joint Center for Life Sciences, School of Life Sciences, Tsinghua University, Beijing 100084, China. [4]State Key Laboratory of Membrane Biology, Institute of Zoology, Chinese Academy of Sciences, Beijing 100101, China. [5]Institute of Stem Cell and Regeneration, Chinese Academy of Sciences, Beijing 100101, China. [6]State Key Laboratory of Environmental Chemistry and Ecotoxicology, Research Center for Eco-Environmental Sciences, Chinese Academy of Sciences, Beijing 100085, China.

Received: 16 November 2019 Accepted: 16 April 2020
Published online: 18 May 2020

References

1. Tadros W, Lipshitz HD. The maternal-to-zygotic transition: a play in two acts. Development. 2009;136:3033–42.
2. Lee MT, Bonneau AR, Giraldez AJ. Zygotic genome activation during the maternal-to-zygotic transition. Annu Rev Cell Dev Biol. 2014;30:581–613.
3. Yartseva V, Giraldez AJ. The maternal-to-zygotic transition during vertebrate development: a model for reprogramming. Curr Top Dev Biol. 2015;113:191–232.
4. Abrams EW, Mullins MC. Early zebrafish development: it's in the maternal genes. Curr Opin Genet Dev. 2009;19:396–403.
5. Chang H, Yeo J, Kim JG, Kim H, Lim J, Lee M, Kim HH, Ohk J, Jeon HY, Lee H, et al. Terminal uridylyltransferases execute programmed clearance of maternal transcriptome in vertebrate embryos. Mol Cell. 2018;70:72–82.e77.
6. Lee MT, Bonneau AR, Takacs CM, Bazzini AA, DiVito KR, Fleming ES, Giraldez AJ. Nanog, Pou5f1 and SoxB1 activate zygotic gene expression during the maternal-to-zygotic transition. Nature. 2013;503:360–4.
7. Vasudevan S, Seli E, Steitz JA. Metazoan oocyte and early embryo development program: a progression through translation regulatory cascades. Genes Dev. 2006;20:138–46.
8. Winata CL, Lapinski M, Pryszcz L, Vaz C, Bin Ismail MH, Nama S, Hajan HS, Lee SGP, Korzh V, Sampath P, et al. Cytoplasmic polyadenylation-mediated translational control of maternal mRNAs directs maternal-to-zygotic transition. Development. 2018;145:dev159566. https://doi.org/10.1242/dev.159566.
9. Giraldez AJ, Mishima Y, Rihel J, Grocock RJ, Van Dongen S, Inoue K, Enright AJ, Schier AF. Zebrafish MiR-430 promotes deadenylation and clearance of maternal mRNAs. Science. 2006;312:75–9.
10. Mishima Y, Tomari Y. Codon usage and 3′ UTR length determine maternal mRNA stability in zebrafish. Mol Cell. 2016;61:874–85.

11. Bazzini AA, Del Viso F, Moreno-Mateos MA, Johnstone TG, Vejnar CE, Qin Y, Yao J, Khokha MK, Giraldez AJ. Codon identity regulates mRNA stability and translation efficiency during the maternal-to-zygotic transition. EMBO J. 2016;35:2087–103.
12. Zhao BS, Wang X, Beadell AV, Lu Z, Shi H, Kuuspalu A, Ho RK, He C. m^{6}A-dependent maternal mRNA clearance facilitates zebrafish maternal-to-zygotic transition. Nature. 2017;542:475–8.
13. Yang Y, Wang L, Han X, Yang WL, Zhang M, Ma HL, Sun BF, Li A, Xia J, Chen J, et al. RNA 5-methylcytosine facilitates the maternal-to-zygotic transition by preventing maternal mrna decay. Mol Cell. 2019;75:1188–1202.e1111.
14. Jain A, Vale RD. RNA phase transitions in repeat expansion disorders. Nature. 2017;546:243–7.
15. Wan Y, Qu K, Zhang QC, Flynn RA, Manor O, Ouyang Z, Zhang J, Spitale RC, Snyder MP, Segal E, Chang HY. Landscape and variation of RNA secondary structure across the human transcriptome. Nature. 2014;505:706–9.
16. Strobel EJ, Yu AM, Lucks JB. High-throughput determination of RNA structures. Nat Rev Genet. 2018;19:615–34.
17. Rouskin S, Zubradt M, Washietl S, Kellis M, Weissman JS. Genome-wide probing of RNA structure reveals active unfolding of mRNA structures in vivo. Nature. 2014;505:701–5.
18. Ding Y, Tang Y, Kwok CK, Zhang Y, Bevilacqua PC, Assmann SM. In vivo genome-wide profiling of RNA secondary structure reveals novel regulatory features. Nature. 2014;505:696–700.
19. Spitale RC, Flynn RA, Zhang QC, Crisalli P, Lee B, Jung JW, Kuchelmeister HY, Batista PJ, Torre EA, Kool ET, Chang HY. Structural imprints in vivo decode RNA regulatory mechanisms. Nature. 2015;519:486–90.
20. Siegfried NA, Busan S, Rice GM, Nelson JA, Weeks KM. RNA motif discovery by SHAPE and mutational profiling (SHAPE-MaP). Nat Methods. 2014;11:959–65.
21. Bevilacqua PC, Ritchey LE, Su Z, Assmann SM. Genome-wide analysis of RNA secondary structure. Annu Rev Genet. 2016;50:235–66.
22. Piao M, Sun L, Zhang QC. RNA regulations and functions decoded by transcriptome-wide RNA structure probing. Genomics Proteomics Bioinformatics. 2017;15:267–78.
23. Sharp PA. The centrality of RNA. Cell. 2009;136:577–80.
24. Pan T, Sosnick T. RNA folding during transcription. Annu Rev Biophys Biomol Struct. 2006;35:161–75.
25. Warf MB, Berglund JA. Role of RNA structure in regulating pre-mRNA splicing. Trends Biochem Sci. 2010;35:169–78.
26. Martin KC, Ephrussi A. mRNA localization: gene expression in the spatial dimension. Cell. 2009;136:719–30.
27. Kozak M. Regulation of translation via mRNA structure in prokaryotes and eukaryotes. Gene. 2005;361:13–37.
28. Garneau NL, Wilusz J, Wilusz CJ. The highways and byways of mRNA decay. Nat Rev Mol Cell Biol. 2007;8:113–26.
29. Mizrahi O, Nachshon A, Shitrit A, Gelbart IA, Dobesova M, Brenner S, Kahana C, Stern-Ginossar N. Virus-induced changes in mRNA secondary structure uncover cis-regulatory elements that directly control gene expression. Mol Cell. 2018;72:862–874.e865.
30. Beaudoin JD, Novoa EM, Vejnar CE, Yartseva V, Takacs CM, Kellis M, Giraldez AJ. Analyses of mRNA structure dynamics identify embryonic gene regulatory programs. Nat Struct Mol Biol. 2018;25:677–86.
31. Han J, Pedersen JS, Kwon SC, Belair CD, Kim YK, Yeom KH, Yang WY, Haussler D, Blelloch R, Kim VN. Posttranscriptional crossregulation between Drosha and DGCR8. Cell. 2009;136:75–84.
32. Vejnar CE, Abdel Messih M, Takacs CM, Yartseva V, Oikonomou P, Christiano R, Stoeckius M, Lau S, Lee MT, Beaudoin JD, et al. Genome wide analysis of 3′ UTR sequence elements and proteins regulating mRNA stability during maternal-to-zygotic transition in zebrafish. Genome Res. 2019;29:1100–14.
33. Sun L, Fazal FM, Li P, Broughton JP, Lee B, Tang L, Huang W, Kool ET, Chang HY, Zhang QC. RNA structure maps across mammalian cellular compartments. Nat Struct Mol Biol. 2019;26:322–30.
34. Charlesworth A, Meijer HA, de Moor CH. Specificity factors in cytoplasmic polyadenylation. Wiley Interdiscip Rev RNA. 2013;4:437–61.
35. Ivshina M, Lasko P, Richter JD. Cytoplasmic polyadenylation element binding proteins in development, health, and disease. Annu Rev Cell Dev Biol. 2014;30:393–415.
36. Laver JD, Li X, Ray D, Cook KB, Hahn NA, Nabeel-Shah S, Kekis M, Luo H, Marsolais AJ, Fung KY, et al. Brain tumor is a sequence-specific RNA-binding protein that directs maternal mRNA clearance during the Drosophila maternal-to-zygotic transition. Genome Biol. 2015;16:94.
37. Gerber AP, Luschnig S, Krasnow MA, Brown PO, Herschlag D. Genome-wide identification of mRNAs associated with the translational regulator PUMILIO in Drosophila melanogaster. Proc Natl Acad Sci U S A. 2006;103:4487–92.
38. Brennan CM, Steitz JA. HuR and mRNA stability. Cell Mol Life Sci. 2001;58:266–77.
39. Mukherjee N, Corcoran DL, Nusbaum JD, Reid DW, Georgiev S, Hafner M, Ascano M Jr, Tuschl T, Ohler U, Keene JD. Integrative regulatory mapping indicates that the RNA-binding protein HuR couples pre-mRNA processing and mRNA stability. Mol Cell. 2011;43:327–39.
40. Zaucker A, Nagorska A, Kumari P, Hecker N, Wang Y, Huang S, Cooper L, Sivashanmugam L, VijayKumar S, Brosens J, et al. Translational co-regulation of a ligand and inhibitor by a conserved RNA element. Nucleic Acids Res. 2018;46:104–19.
41. Gilligan PC, Kumari P, Lim S, Cheong A, Chang A, Sampath K. Conservation defines functional motifs in the squint/nodal-related 1 RNA dorsal localization element. Nucleic Acids Res. 2011;39:3340–9.
42. Li X, Lu YC, Dai K, Torregroza I, Hla T, Evans T. Elavl1a regulates zebrafish erythropoiesis via posttranscriptional control of gata1. Blood. 2014;123:1384–92.
43. Lebedeva S, Jens M, Theil K, Schwanhausser B, Selbach M, Landthaler M, Rajewsky N. Transcriptome-wide analysis of regulatory interactions of the RNA-binding protein HuR. Mol Cell. 2011;43:340–52.
44. Harvey SA, Sealy I, Kettleborough R, Fenyes F, White R, Stemple D, Smith JC. Identification of the zebrafish maternal and paternal transcriptomes. Development. 2013;140:2703–10.
45. Eckersley-Maslin MA, Alda-Catalinas C, Reik W. Dynamics of the epigenetic landscape during the maternal-to-zygotic transition. Nat Rev Mol Cell Biol. 2018;19:436–50.
46. Taliaferro JM, Lambert NJ, Sudmant PH, Dominguez D, Merkin JJ, Alexis MS, Bazile C, Burge CB. RNA sequence context effects measured in vitro predict in vivo protein binding and regulation. Mol Cell. 2016;64:294–306.
47. Lewis CJ, Pan T, Kalsotra A. RNA modifications and structures cooperate to guide RNA-protein interactions. Nat Rev Mol Cell Biol. 2017;18:202–10.